Electronic Supporting Information for

Direct Realization of an Operando Systems Chemistry Algorithm (OSCAL) for powering Self-Propelled Nanomotors

Apabrita Mallick[a], Shounik Paul[a], Teng Ben*[b], Shilun Qiu[b], Francis Verpoort*[c, d, e] and Soumyajit Roy*[a]

[a]Eco-Friendly Applied Materials Laboratory (EFAML), Materials Science Centre, Department of Chemical Sciences, Mohanpur Campus, Indian Institute of Science Education and Research, Kolkata,741246, West Bengal, India. Email: s.roy@iiserkol.ac.in

[b]Department of Chemistry, Jilin University, Changchun 130012, China.

E-mail: tben@jlu.edu.cn

[c]LOCOM, State Key Laboratory of Advanced Technology for Materials Synthesis and Processing, Wuhan University of Technology, 430070 Wuhan, P.R. China.

[d]Ghent University - Global Campus Songdo, 119 Songdomunhwa-Ro, Ywonsu-Gu, Incheon, Republic of Korea. Email: francis.verpoort@ugent.be

[e]National Research Tomsk Polytechnic University, Lenin Avenue 30, 634050 Tomsk, Russian Federation.

Contents

1. Characterization of the nanocarpets 3
3. Comparison of the nanocarpets before and after catalysis 10
4. References 15

1. Characterization of the nanocarpets:

A. SEM imaging, EDS and DLS studies

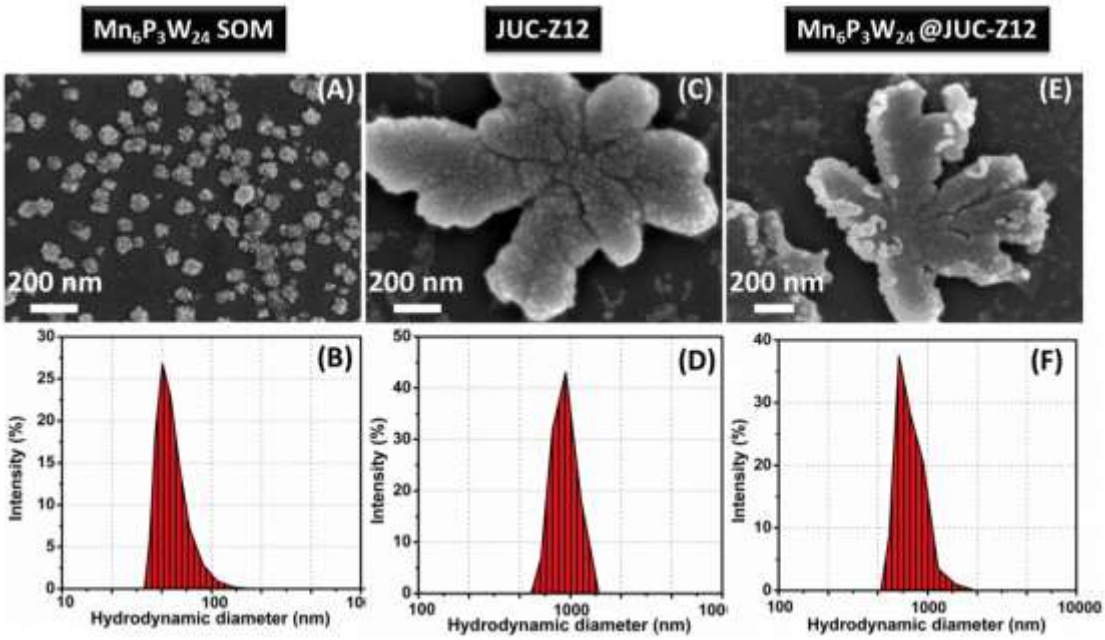

Figure S1: (A) SEM image and (B) DLS of {$Mn_6P_3W_{24}$} SOM, (C) SEM image and (D) DLS of JUC-Z12, (E) SEM image and (F) DLS of SOM-JUC-Z12

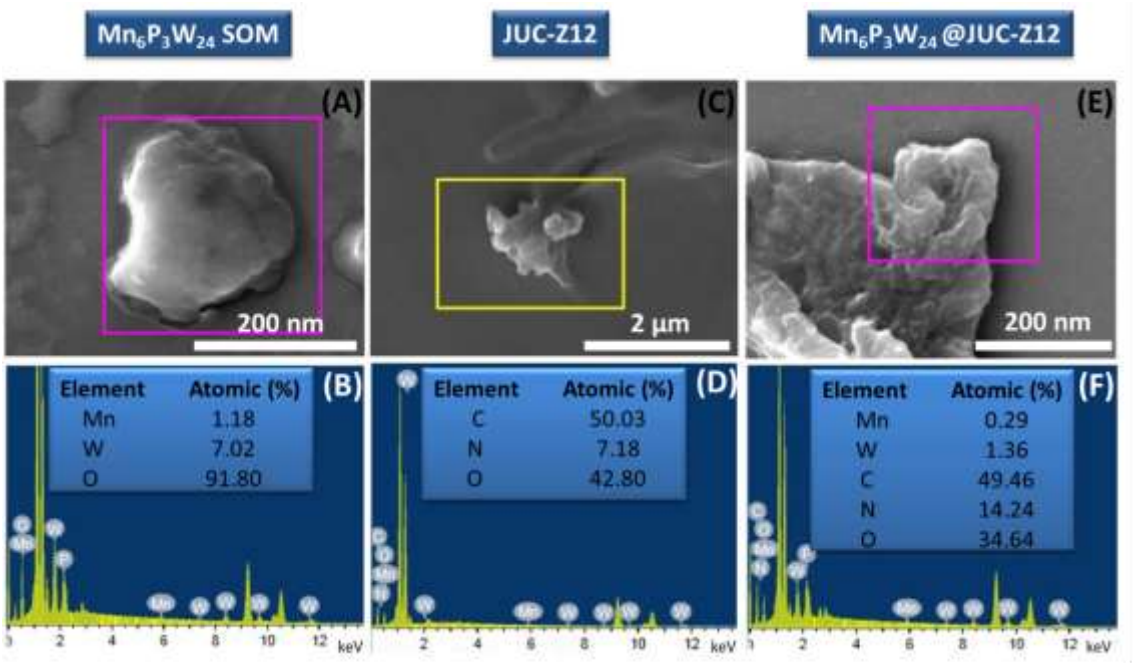

Figure S2: EDS studies showing atomic % of constituent atoms in (A) and (B) {$Mn_6P_3W_{24}$} SOM, (C) and (D) JUC-Z12, (E) and (F) SOM-JUC-Z12.

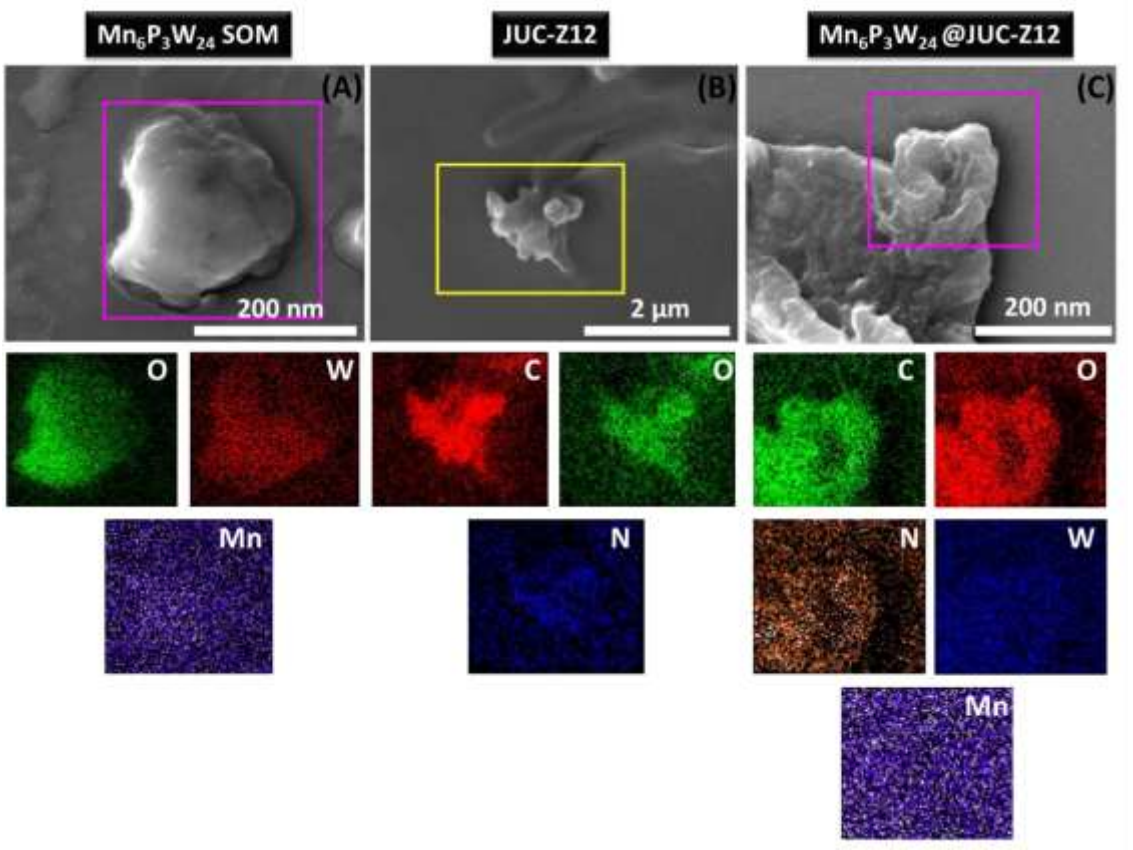

Figure S3: EDS mappings of the constituent atoms in (A) {$Mn_6P_3W_{24}$} SOM, (B) JUC-Z12 and (C) SOM-JUC-Z12.

B. HATR-IR and PXRD studies

The characteristic HATR-IR (Fig. S4) peaks of the composite at 1031 (P-O stretching), 938 (W=O stretching), 878 (W-O-W stretching), 737 (Mn-O-Mn stretching) and 485 cm^{-1} (Mn-O bending) attribute to $\{Mn_6P_3W_{24}\}$ SOM and confirms that all peaks of the SOM are retained in SOM-POF composite. The presence of bands at 1633 (water in the dispersion, C=O and C=N stretching), 1418 (benzimidazole ring), 1299 cm^{-1} (C-N stretching) arise due to JUC-Z12.

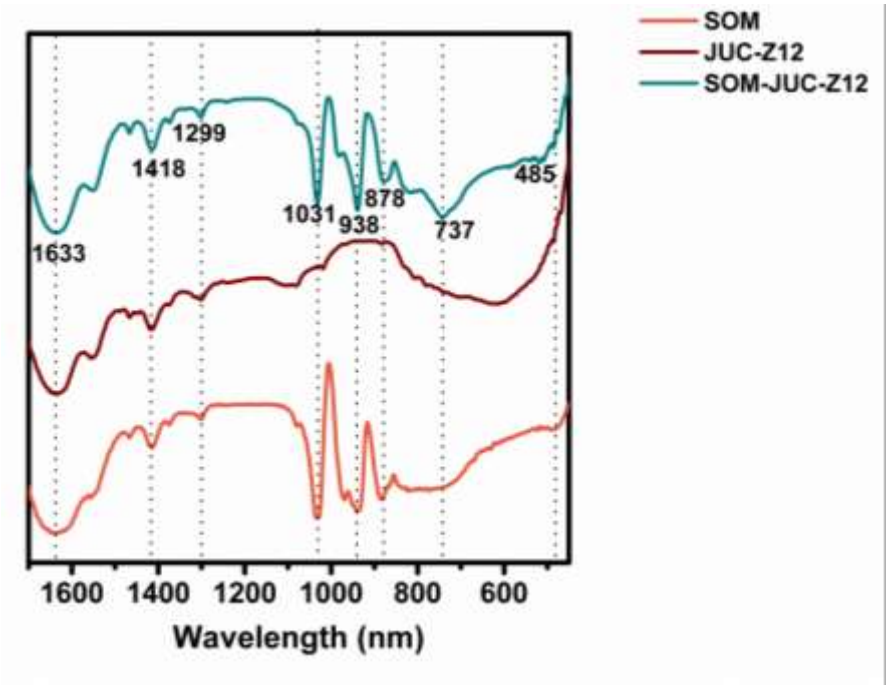

Figure S4: HATR-IR spectra of $\{Mn_6P_3W_{24}\}$ SOM, JUC-Z12 and SOM-JUC-Z12.

HRTEM and PXRD (obtained from extracted solid) studies from literature suggest that JUC-Z12 is amorphous in nature as no crystalline planes have been observed. When SOMs are incorporated into the micropores of JUC-Z12, some very small peaks are observed from PXRD (Fig. S5) which correspond to the [3,2,-2], [0,6,1] and [2,5,7] planes of the POM; $Na_{17}[Mn_6P_3W_{24}O_{94}(H_2O)_2].43H_2O$ thus affirming the supramolecular composite formation.

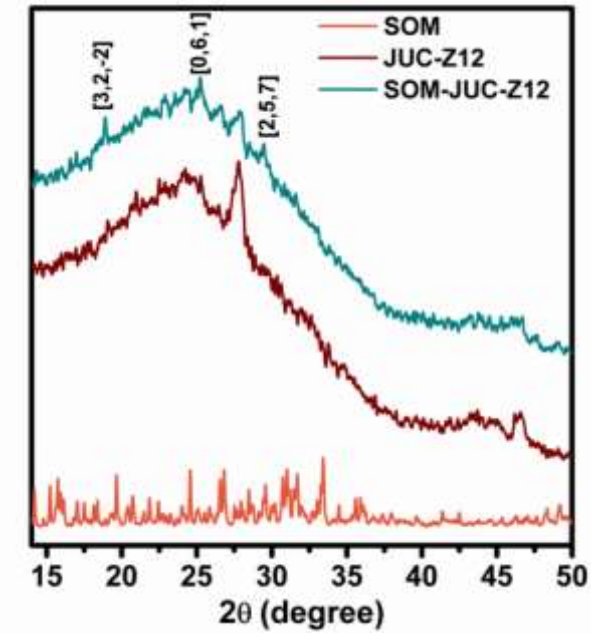

Figure S5: PXRD spectra of {$Mn_6P_3W_{24}$} SOM, JUC-Z12 and SOM-JUC-Z12.

C. Gas sorption studies

BET studies (Fig. S6) also support the impregnation of SOMs into the micropores as the pore size distribution (Fig. S6c) obtained from BET show that the micropores (1.09 nm) present in JUC-Z12[1] are now blocked in the {$Mn_6P_3W_{24}$}-JUC-Z12 composite. Also, the N_2 adsorption curve of JUC-Z12 alone shows a sharp uptake in the low pressure region[1] due to its microporous structure whereas no such sharp uptake of N_2 has been noticed in the adsorption curve (Fig. S6a) of SOM-JUC-Z12 indicating that the micropores are now blocked by the {$Mn_6P_3W_{24}$} SOMs, whereas the mesopores (>2 nm) of the JUC-Z12 remain vacant in the composite. This hierarchical mesoporous structure of the SOM-JUC-Z12 facilitates chemical reactions on its surface making the structure suitable for creating the swimming nanorafts. From the gas sorption studies the BET surface area of the composite was calculated to be (126.643±1.345) $m^2 g^{-1}$ (Fig. S6c) which is much less than the BET surface area, 750 $m^2 g^{-1}$

of JUC-Z12 only. The surface area of the SOM-JUC-Z12 composite is almost 6 times less as compared to JUC-Z12 alone which implicates the incorporation of the SOMs into JUC-Z12.

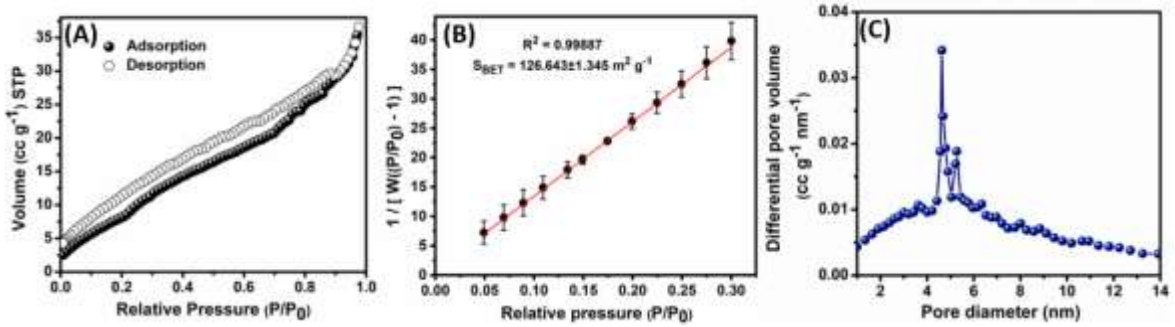

Figure S6: (A) N_2 sorption isotherms of SOM-JUC-Z12, solid symbols denote adsorption and open symbols denote desorption. (B) BET plot. Error bars represent standard deviations from three repeated experiments. (C) Pore size distributions derived from N_2 adsorption isotherm.

D. Potentiodynamic studies

Potentiodynamic studies have been performed with SOM-JUC-Z12 at different scan rates (50-500 mV s^{-1}). The current densities of the oxidation (E_{ox} = 0.775 V) and reduction (E_{red} = 0.37 V) peaks follow a linear trend suggesting the process is adsorption controlled. These electrochemical studies strongly suggest the formation of a supramolecular host-guest complex, SOM-JUC-Z12.[2]

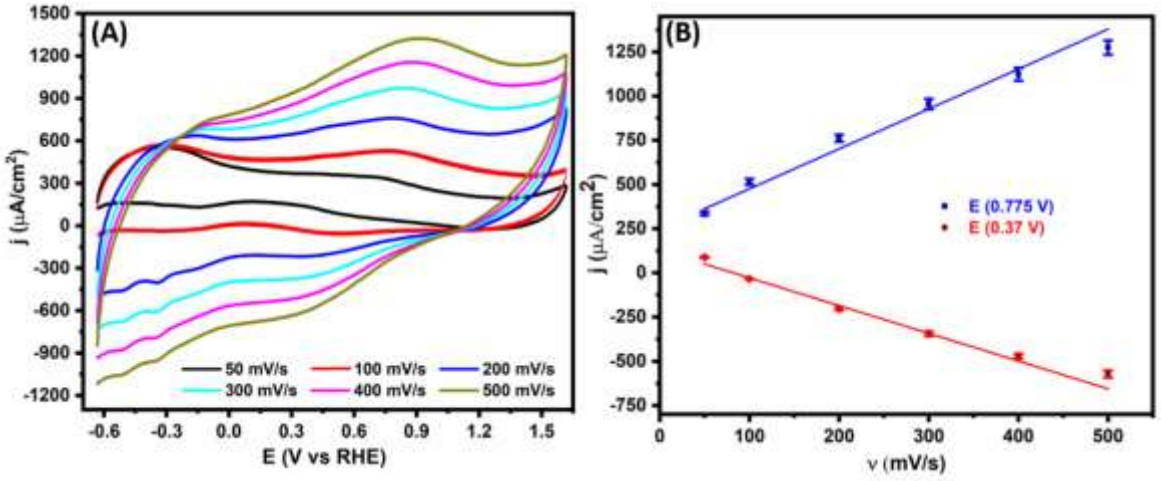

Figure S7: (A) Cyclic voltammetry studies of SOM-JUC-Z12 at scan rates of i. 50, ii. 100, iii. 200, iv. 300, v. 400 and vi. 500 mV/s. (B) Plot of peak current density vs scan

rate. Blue represents the oxidation current densities and red represents the reduction current densities respectively. Error bars represent standard deviations from four sets of repeated measurements.

E. Association constant and free energy of association between SOM and JUC-Z12 from UV-Vis titration

To quantify the supramolecular interaction between the host (JUC-Z12) and the guest (SOM) we have calculated the association constant (K_a) and free energy of association (ΔG_a) by using UV-Vis titration.[3] The experimental details of UV-Visible titration are described in the Experimental Section of the modified manuscript. From the UV-Visible spectroscopic titration in the modified Supporting Information (Section 1E: Association constant and free energy of association between SOM and JUC-Z12 from UV-Vis titration, Figure S8A) it is evident that the absorbance (A) of the main absorption peak (λ_{max} = 277 nm) of JUC-Z12 is enhanced with gradual addition of aliquots of SOMs. Maximum absorbance is reached on addition of 160 µL of SOM (concentration of SOM= 0.03 µM). Beyond this point, the absorbance decreases with further addition of SOMs. As the SOMs begin to load into the micropores of JUC-Z12 the absorbance starts increasing, reaches the critical point when all the loading sites of JUC-Z12 are completely occupied and the system reaches a dynamic equilibrium.[4] Beyond this critical point, the absorbance starts tipping down due to presence of unbound SOMs in the solution. The data from UV-Vis titration was analysed using the linear regression method, Benesi-Hildebrand[5] to find out the association constant between SOMs and JUC-Z12. Bensei-Hildebrand equation is represented as follows:[6]

$$\frac{A_{max}}{A_{max} - A} = \frac{1}{K_a . [G]}$$

where, A_{max} is the absorbance at the tipping point (160 µL), A is the absorbance of the individual SOM-JUC-Z12 complex at 277 nm, K_a is the association constant and $[G]$ is the concentration of the guest, i.e.; SOM. From the linear fit of $\frac{A_{max}}{A_{max}-A}$ vs $\frac{1}{[G]}$, the value of K_a is

(3.681±0.281) X 10^{11} M^{-1} (Supporting Information, Figure S8B). The free energy of association (ΔG_a) is -85.9 kJ which quantitatively describes the strength of binding of SOMs with JUC-Z12.

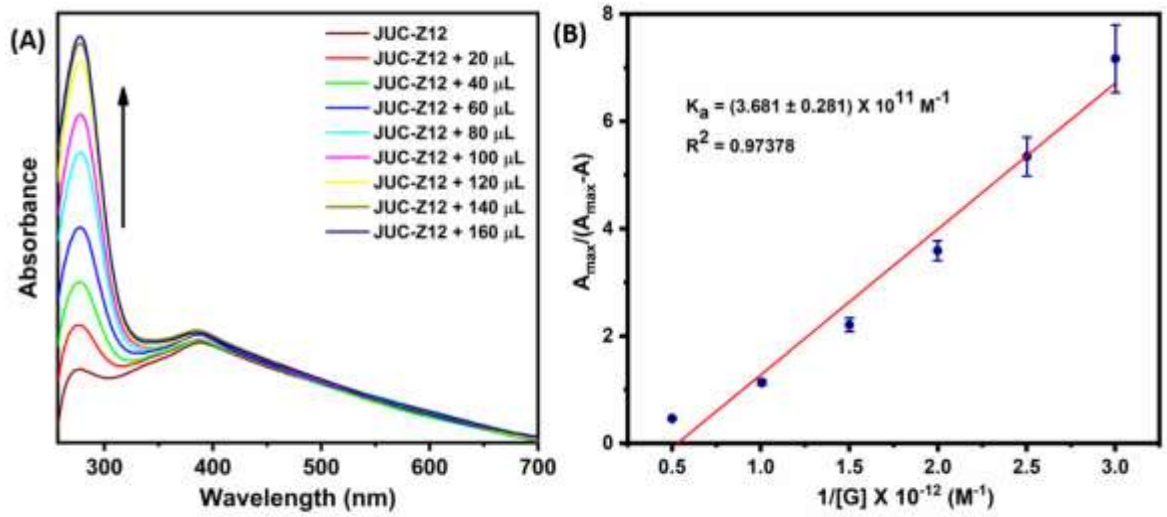

Figure S8: (A) UV-Visible absorbance titration of JUC-Z12 with SOM. (B) Benesi-Hildebrand plot for calculation of association constant K_a (λ_{max} = 277 nm). Error bars represent standard deviations from a set of five repeated experiments.

2. Comparison of the nanocarpets before and after catalysis with MeOH and 0.5 M H_2SO_4

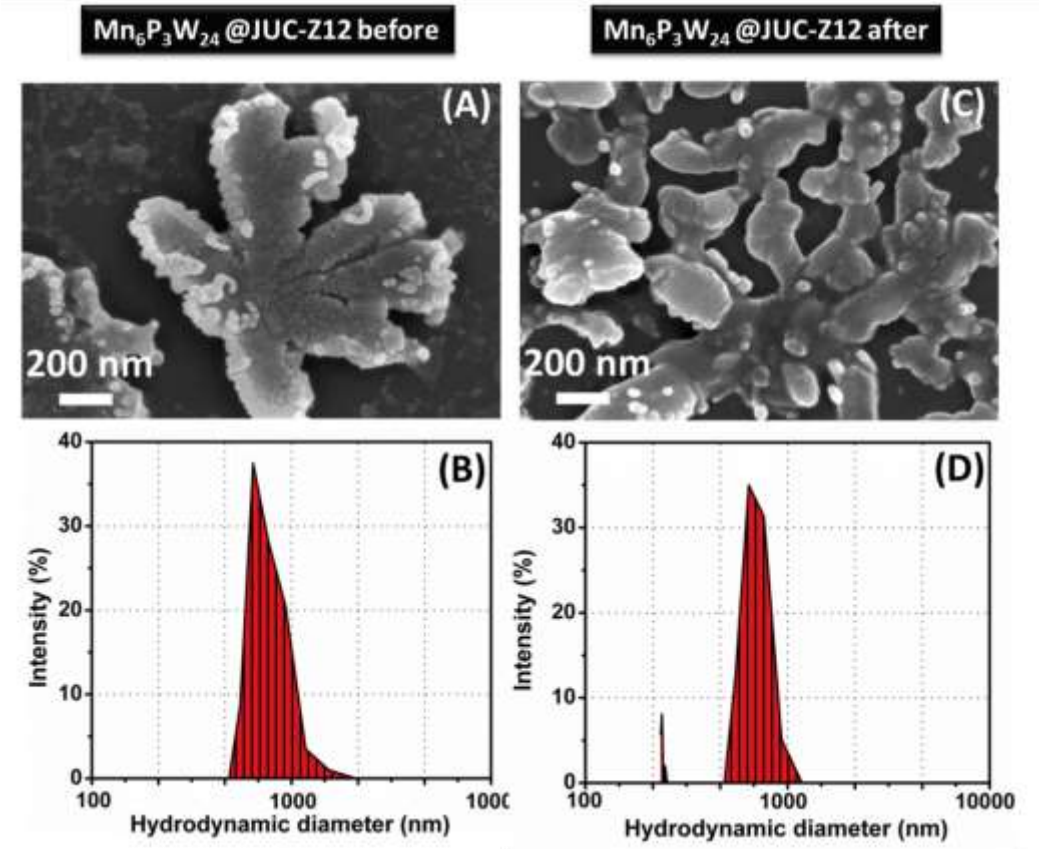

Figure S9: (A) SEM image and (B) DLS studies of SOM-JUC-Z12 before reaction and (A) SEM image and (B) DLS studies of SOM-JUC-Z12 after reaction with MeOH and 0.5 M H_2SO_4.

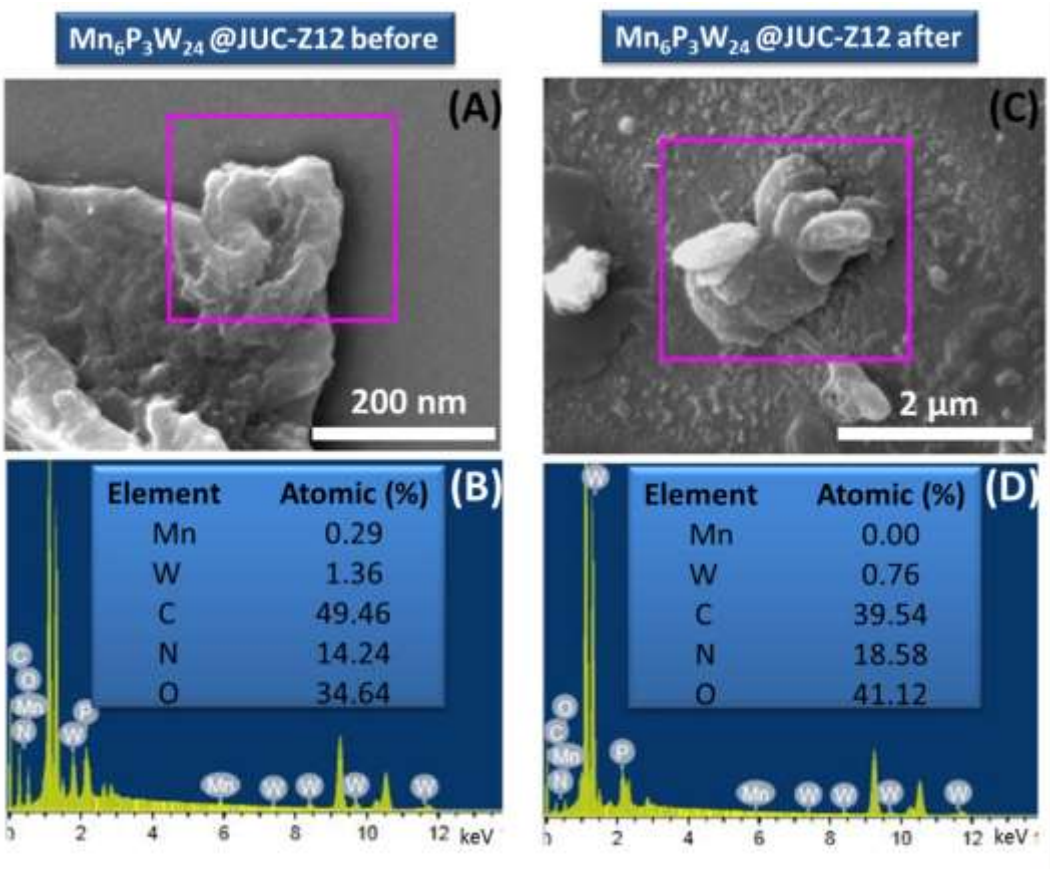

Figure S10: EDS studies showing atomic % of constituent atoms in (A) and (B) SOM-JUC-Z12 before reaction, (C) and (D) SOM-JUC-Z12 after reaction with MeOH and 0.5 M H_2SO_4.

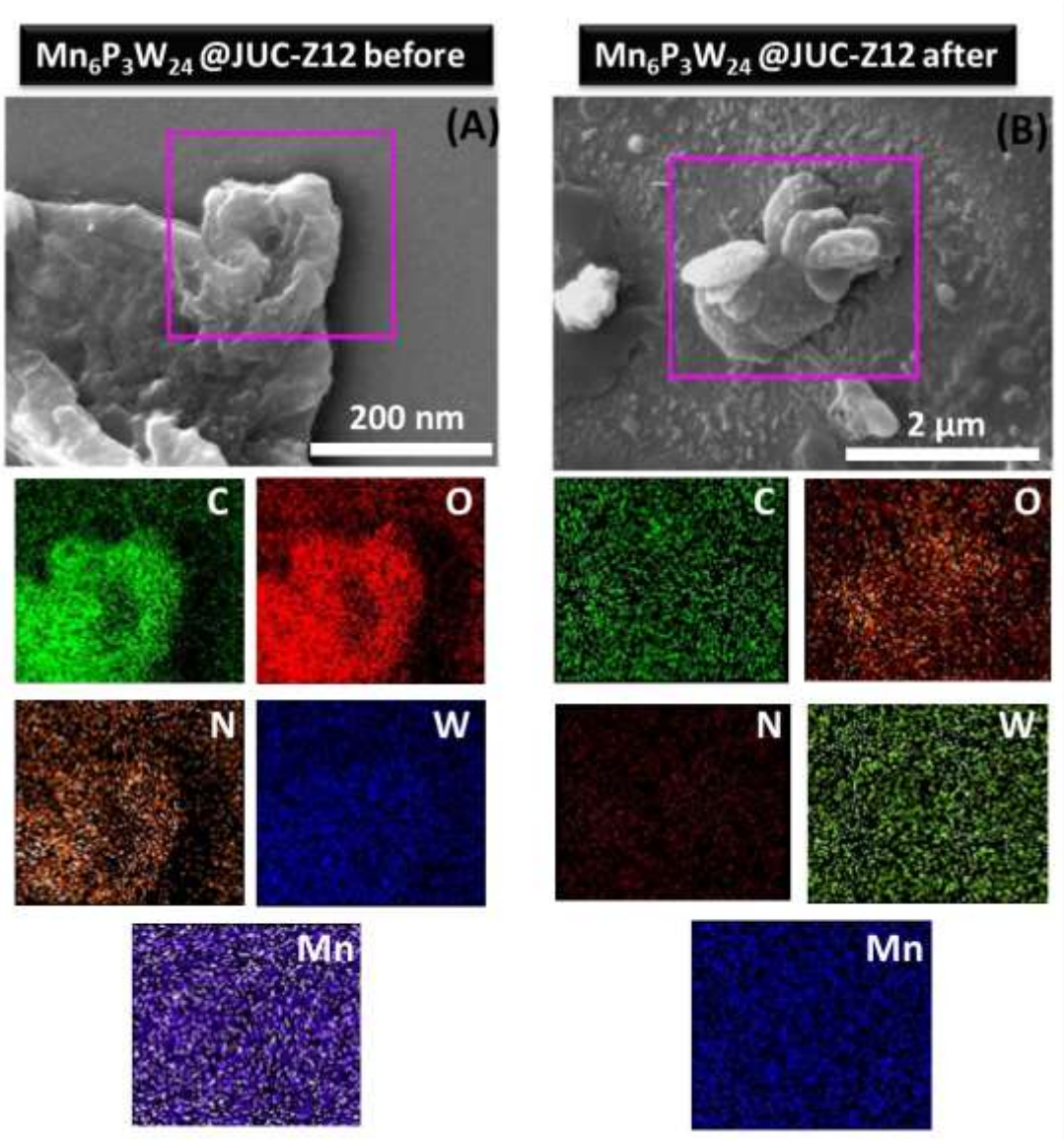

Figure S11: EDS mappings of the constituent atoms in (A) SOM-JUC-Z12 before reaction, (B) SOM-JUC-Z12 after reaction with MeOH and 0.5 M H_2SO_4.

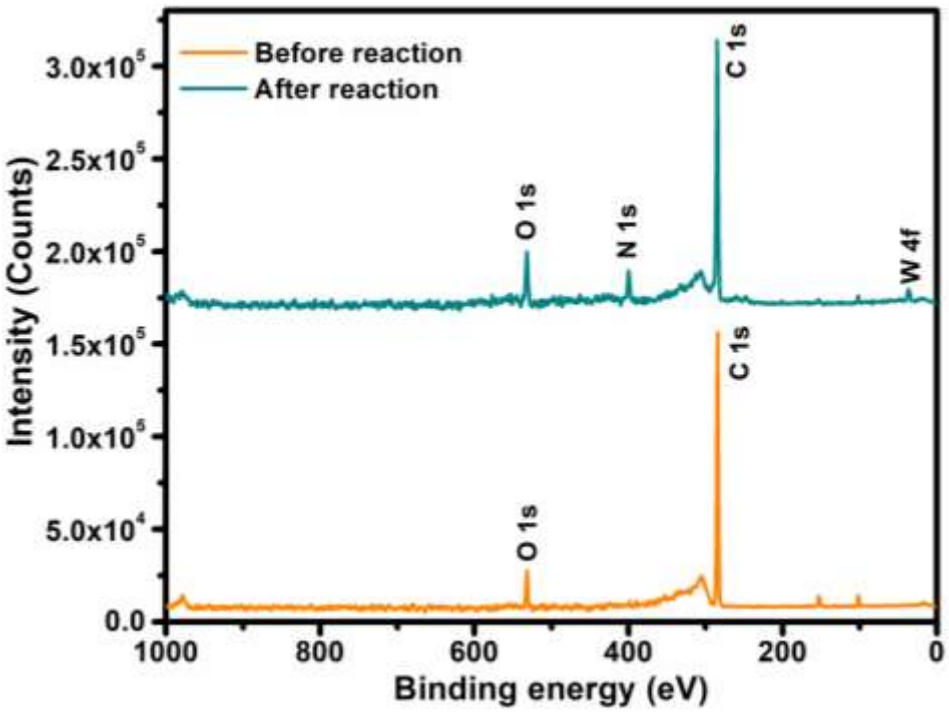

Figure S12: XPS Survey scan of SOM-JUC-Z12 before and after reaction with MeOH and 0.5 M H_2SO_4.

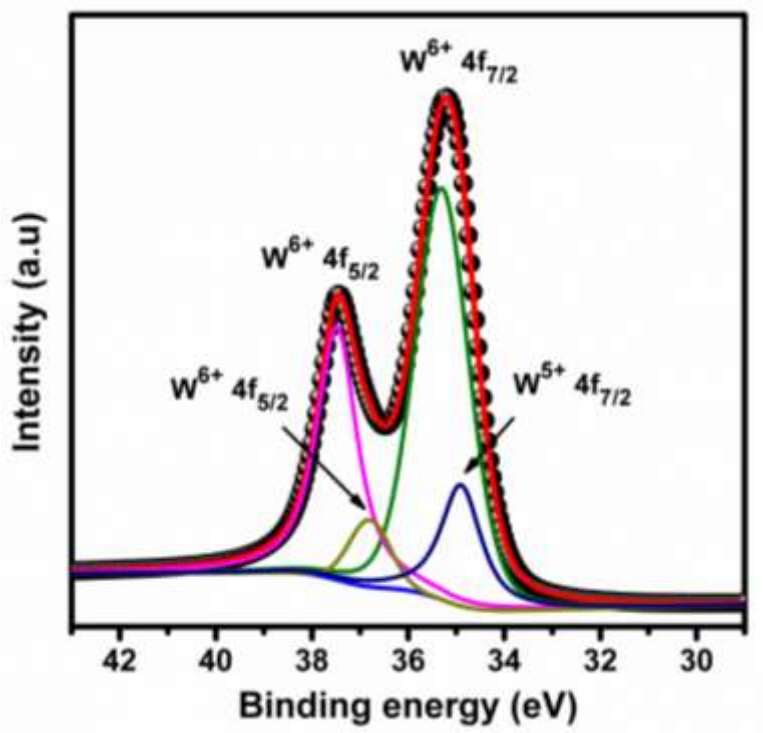

Figure S13: Deconvoluted core level XPS spectra of W 4f in SOM-JUC-Z12 post reaction with MeOH and 0.5 M H_2SO_4.

The W 4f core level spectra (Fig. 2k) obtained post reaction corresponds to two different charge states as the spectra consist of two doublets. The intense doublet with peak positions of W $4f_{7/2}$ at 35.3 eV and W $4f_{5/2}$ at 37.4 eV affirm the presence of W^{6+}. The second doublet with peak positions of W $4f_{7/2}$ at 34.6 eV and W $4f_{5/2}$ at 36.9 eV correspond to W^{5+}. The peak ratios of W $4f_{7/2}$: W $4f_{5/2} \approx 4/3$, peak positions (ΔBE (W $4f_{7/2}$ – W $4f_{5/2}$)) = 2.1-2.3 eV were maintained for both oxidation states. The peak areas of W $4f_{7/2}$ for W^{6+} and W^{5+} are 80% and 20% respectively of the total W 4f signal.

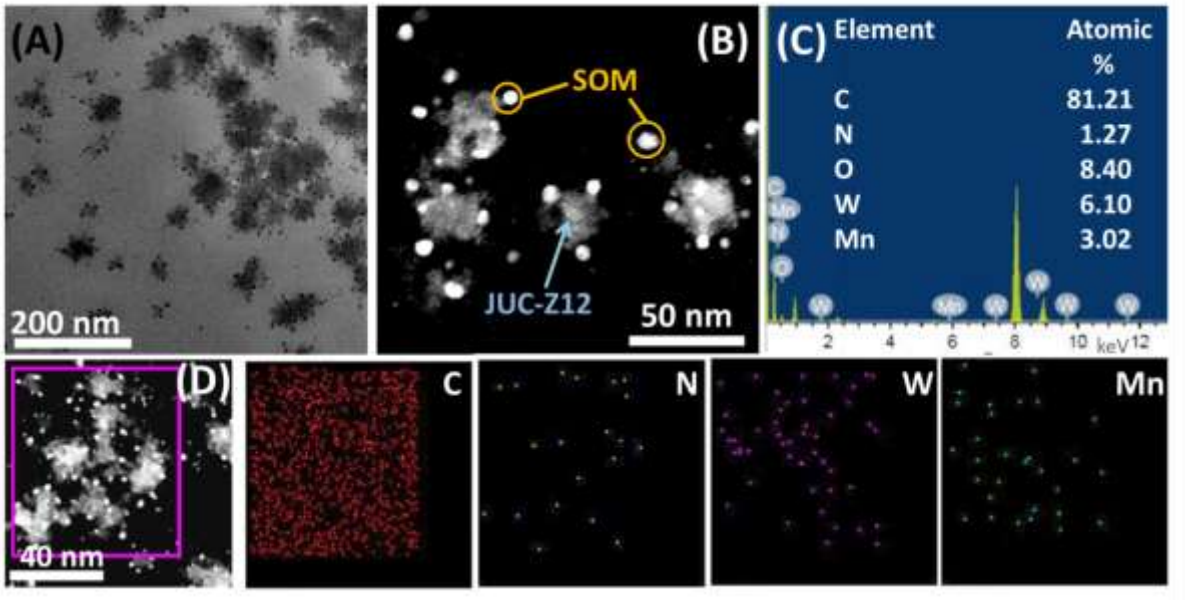

Figure S14: (A) TEM image, (B) HAADF-STEM, (C) EDS showing atomic % and (D) EDS mapping of constituent atoms of SOM-JUC-Z12 after reaction with MeOH and 0.5 M H_2SO_4.

SEM images (Fig. S9c) of SOM-JUC-Z12 after reaction show that a number of SOMs are scattered randomly on JUC-Z12 surface. TEM images (Fig. 2e and 2f) of SOM-JUC-Z12 recorded after separating them from the fuel reveal that the spherical dark SOM particles are clustered around the edges of JUC-Z12. EDS (Fig. 2d and 2h, Fig. S10 and S11) results from both SEM and TEM show that after reaction, the atomic % of both Mn and W increase when

compared with the atomic % of the same before reaction. This atomic % increase of the SOM constituents supports that the SOMs get released from the pores of JUC-Z12 and spread out on its surface and as EDS is recorded on the surface of the particles, the atomic % is more in this case as compared to impregnated SOMs. All these experimental evidences support the proposed mechanism of propulsion of the nanorafts by release and reorganization of SOMs.

3. References

1. B. Liu, T. Ben, J. Xu, F. Deng and S. Qiu, *New Journal of Chemistry*, 2014, **38**, 2292-2299.
2. M. Palomar-Pardavé, S. Corona-Avendaño, M. Romero-Romo, G. Alarcón-Angeles, A. Merkoçi and M. Ramírez-Silva, *Journal of Electroanalytical Chemistry*, 2014, **717**, 103-109.
3. P. Thordarson, *Chemical Society Reviews*, 2011, **40**, 1305-1323.
4. L. Wang, Z. Zhang, M. Li, Q. Li, B. Wang, S. Wang, H. Zhou and B. Mao, *ChemCatChem*, 2020, **12**, 2469-2477.
5. A. K. Nair, P. P. Neelakandan and D. Ramaiah, *Chemical communications*, 2009, **42**, 6352-6354.
6. T. A. Khan, M. Sheoran, S. Jain, D. Gupta and S. G. Naik, *Spectrochimica Acta Part A: Molecular and Biomolecular Spectroscopy*, 2018, **189**, 176-182.